Fabrication of n-ZnO/p-Si++ Hetero-junction Devices for Hydrogen Detection: Effect of Annealing Temperature

Vinod Kumar
SRMIST: SRM Institute of Science and Technology
Ishpal Rawal (rawal92@gmail.com)
University of Delhi https://orcid.org/0000-0002-7053-3625
Vipin Kumar
SRMIST: SRM Institute of Science and Technology

Research Article

Keywords: ZnO thin films, Hydrogen sensing, Freundlich's isotherm, Hetero-junctions

Posted Date: September 15th, 2021

DOI: https://doi.org/10.21203/rs.3.rs-891721/v1

Version of Record: A version of this preprint was published at Silicon on November 12th, 2021. See the published version at https://doi.org/10.1007/s12633-021-01508-3.

Fabrication of n-ZnO/p-Si^{++} hetero-junction devices for hydrogen detection: Effect of annealing temperature

Vinod Kumar[1], Ishpal Rawal[2*], Vipin Kumar[1]
[1]Department of Electronics and Communication Engineering, SRM-Institute of Science and Technology, Ghaziabad, UP-201204, India
[2]Department of Physics, Kirori Mal College, University of Delhi, Delhi-110007

Abstract

In the present study, we reports the fabrication of n-ZnO/p-Si^{++} hetero-junction devices for the detection of hydrogen leakage in ambient air environment. For the fabrication of n-ZnO/p-Si^{++} hetero-junction devices, high quality ZnO thin films are grown by controlled thermal evaporation technique on the highly doped p-type silicon substrates at 400 ^{o}C. The two sets of films deposited at 400 ^{o} C are further annealed at 500 and 600 ^{o}C to examine the effect of annealing temperature on the structural, morphology, electrical and gas sensing properties of the deposited films. It is revealed from the x-ray diffraction studies that the crystallite size, and the density of the films increase from 22.55 to 24.95 nm, from 5.65 to 5.68 g/cm^3, respectively, on increasing the fabrication temperature from 400 to 600 ^{o}C. In contrast to it, the grain boundary specific surface area decrease from 8.79 x10^7 to 7.88 x10^7 m^{-1} on changing the fabrication temperature from 400 to 600 ^{o}C. The hydrogen gas sensing response of the fabricated devices has also been recorded at different operating temperatures and different hydrogen concentrations (200 to 1000ppm) in air ambient. It is found that the gas sensing response of the fabricated devices increase with increase in operating temperature (up to 100 ^{o}C) and decease beyond this temperature. The gas sensing responses of the devices fabricated at 400, 500 and 600 ^{o}C are found to be 97.22, 64.23 and 40.77 % at 1000 ppm of hydrogen. A decrease in gas sensing response with fabrication temperature is attributed to the increase in crystallite size (quantum size effect), density of films (i.e. lower penetration) and decrease in grain boundary specific surface area (i.e. active sites) with annealing temperature. The mechanism of the gas sensing in these devices has also been systematically analyzed under different models.

Keywords: ZnO thin films, Hydrogen sensing, Freundlich's isotherm, Hetero-junctions

Corresponding author: rawal92@gmail.com, rawalishpal@gmail.com (I. Rawal)

1. Introduction

Hetero-junction devices always remain the center of attention for their eclectic range of applicability in rectifying diodes, lasing devices, photodetectors, light emitting diodes and transistors, etc [1-5]. However, for a longer time, these optoelectronic devices remained dependent on a costly and sophisticated silicon based technology. In contrast to this, in recent years, metal oxide based hetero-junction devices received significant attention because of their low cost, easy and eco-friendly fabrication technologies [3-7]. Apart from the optoelectronic applications of the metal oxide based hetero-junctions, the gas sensing devices have shown augmented device performances towards many hazardous gases [6,7]. This includes detection of H_2S, chloroform, ammonia, CO_2, NO_2, NH_3 and the most vulnerable hydrogen gas [7,8]. However, hydrogen finds diverse range of utility in health sectors, nuclear power plants, and as a highly clean and sustainable renewable source of energy of automobile industries and space exploration [9, 10]. In spite of these sundry applications, hydrogen is the most vulnerable for human being because of its colorlessness, odorlessness, highly inflammable and explosive nature [11] Thus, to avoid any serious accident, the continuous monitoring of hydrogen at low ppm levels is essential. Researchers are continuously exploring for highly sensitive, stable and robust sensing elements to trace out the leakage of hydrogen in working environment. A variety of metal oxide based semiconductors are widely studied for the detection of wide range of gases. Out of these metal oxide semiconductors, zinc oxide (ZnO) is an intrinsically n-type semiconductor, which was first time used by Seiyama et al. [12] for the detection of flammable gases in thin film form. Henceforth, ZnO thin films were utilized for the detection of variety of gaseous by numerous researchers in different modular forms such as MOS capacitors, Schottky diodes, MOSFETs, simple resisters, etc [13,14]. Ominously, the pristine ZnO thin films have poor

hydrogen detection ability. These films generally have higher operating temperature and low sensitivity and selectivity for hydrogen. Therefore, different device fabrication strategies and methods have been employed to enhance the sensing ability of ZnO for hydrogen gas. This includes the decoration of ZnO by noble metals, doping and formation of nanocomposites of ZnO with different metal oxide and post deposition treatments, [11,14] etc. The hetero-junction device based on metal oxides (particularly ZnO) is one of such choices that can be employed for enhancing the device performance. It is reported that fabrication of metal oxide hetero-junction devices decrease the possibility of electron-hole recombination by altering the charge transfer process and electronic structure of the device, and hence improved the gas sensing performance [15-17]. Therefore, in the present study, the hetero-junctions of n-ZnO/p-Si are fabricated by thermal evaporation technique at 400 ^{o}C. The post-deposition heat treatment has also been done at 500 and 600 ^{o}C to investigate the effect of annealing temperatures on the sensing ability of the fabricated devices towards hydrogen gas. The effect of annealing temperature on the structural and morphological properties has also been investigated.

2. Experimental details

2.1. Growth of n-ZnO thin films

The n-type ZnO (n-ZnO) thin films were grown by simple thermal evaporation technique on the heavily doped p-type silicon substrates at a substrate temperature of 400 ^{o}C. For the deposition of high quality n-ZnO thin films, the high purity (99.99%) ZnO dust was thermally evaporated under constant vacuum condition (3.2 x10^{-3} mbar) maintained through a continuous flow of well-prepared mixture of argon (80%) and oxygen (20%). Before the deposition of n-ZnO thin films, a base vacuum of ~2.1 x10^{-5} mbar was achieved in the deposition chamber with the help of diffusion and rotary pumps. The precursor material, ZnO powder, was placed in a

molybdenum boat, which was maintained at a distance of 12 cm from the substrate holder. The substrates were heated to a temperature of 400 ^{o}C using a substrate heater attached with the substrate holder. The ZnO powder was slowly evaporated by passing a low current for 30 minutes and the thickness of the films was constantly supervised using the thickness monitor fixed with sample holder. After achieving the thickness of ~250 nm of the ZnO thin films, evaporation process was stopped and the substrates were left to cool naturally inside the deposition system and taken out next day. The deposition of n-ZnO thin films on p-Si^{++} substrates result into the fabrication of n-ZnO/p-Si^{++} hetero-junction devices. Out of several deposited samples, two sets of thin films were further annealed at 500 and 600 ^{o}C to examine the effect of heat treatment on the properties of the deposited thin films. These three sets of n-ZnO/p-Si^{++} thin films were designated as n-ZnO/p-Si^{++} at 400 ^{o}C, n-ZnO/p-Si^{++} at 500 ^{o}C, and n-ZnO/p-Si^{++} at 600 ^{o}C, respectively.

Characterization of deposited thin films

The structural and phase analysis of the deposited thin films was carried out using x-ray diffractometer (D8 discover), ASX-Bruker made. The surface examination was done with the help of high resolution field emission scanning electron microscopy, Gemini-500, Zeiss, Germany. The conduction behavior of the charge carrier in air and hydrogen (H_2) ambients was examined using the Keithley's 2410 source measure unit. The current-voltage (I-V) characteristics of all three sets of films were recorded in sandwich structure Pt/n-ZnO/p-Si^{++}/Pt. The Pt electrodes of ~50 nm were deposited on both sides of the hetero-junction devices. The room temperature I-V measurements were performed in ambient air and hydrogen environments. The transient hydrogen gas sensing measurements on all three sets of hetero-junction devices were performed at 100 ^{o}C at different concentrations (200,400, 600,800 and 1000 ppm) of hydrogen gas using Keithley's 2410 source measure unit.

3. Results and Discussion

3.1. Structural and morphological studies

Figure 1(a) shows the XRD patterns of the ZnO thin films, consist of various sharp reflections located at 31.73, 34.44, 36.24, 47.51, 56.56, 62.79, and 67.99^{o}, which are related with the polycrystalline (hkl) planes (100), (002), (101), (102), (110), (103) and (112), respectively [2,18,19]. These peak positions related with different (hkl) planes are well corroborated with JCPDS Card No. 36-1451, 15-17 corresponding to the hexagonal wurtzite structure of ZnO. All these peaks are purely associated with the highly quality ZnO and thus, negate the possibility of any impurity present in the deposited films. The n-ZnO thin film deposited at 400 ^{o}C has been further annealed at 500 and 600 ^{o}C to investigate the effect of heat treatment on the structural and other properties of the deposited film. The structural change in the deposited film can be examined in terms of various structural parameters like crystallite size (Δ), lattice parameters 'a' and 'c', stress and strain, volume of the unit cell and density of the deposited film. Therefore, these structural parameters have been evaluated for all three sets of films. The well known Debye-Scherrer's formula [18-21] given below is used to determine the crystallite size,

$$\Delta = \frac{0.91\lambda}{\beta\cos\theta} \quad (1)$$

Where, λ is the wavelength (~1.5406Å) of CuKα source used for the irradiation of the films and, θ is the angular position of a particular plane used for the determination of crystallite size and β is the full width at half maximum of the corresponding peaks of the plane measured in radians. The average crystallite sizes for n-ZnO thin films grown at 400, 500 and 600 ^{o}C are found be ~ 22.55, 23.88 and 24.95 nm, respectively. It is observed that the crystallite size of the deposited film at 400 ^{o}C increases slightly with increase in annealing temperature to 500 and 600 ^{o}C. This is because of that the annealing temperature provides the necessary energy for crystallization and

adjustment of atoms/molecules of the film for the formation long order crystal structure. The calculated average crystallite sizes for the deposited films are further used to examine the average defect density in the films using the relation [18,19]

$$\delta = \frac{1}{\Delta^2} \quad (2)$$

It is found that the average defect density for the deposited ZnO film deposited at 400 ^{o}C decreases 1.97x10^{15} to 1.75 x10^{15} and to 1.61 x10^{15} m^{-2} with increase in annealed temperature to 500 and to 600 ^{o}C, respectively. The decrease in defect density with increase in annealing temperature suggests the increase in the quality of the deposited film with heat treatment. The observed values of the defect density for the present thin films are in the range of reported values for ZnO thin films [19,20].

The inter-planer spacing (d) for the deposited films has been estimated by utilizing the well-known Bragg's law

$$2d\sin\theta = n\lambda \quad (2)$$

Where, symbols have their usual meanings. The obtained values of the d-spacing for the (hkl) plane (002) are found to be 2.605, 2.602, and 2.601Å for the films heat treated at 400, 500 and 600 ^{o}C, respectively. A slight decrease in inter-planer spacing with increase in annealing temperature can be attributed to the re-arrangement/adjustment of atoms at higher temperature due to presence of sufficient energy for crystallization.

The obtained values of the d-spacing are further used to estimate lattice parameters 'c' and 'a' [22] using the relations

$$\frac{1}{d_{hkl}^2} = \frac{4}{3}\left(\frac{h^2+hk+k^2}{a^2}\right) + \left(\frac{l^2}{c^2}\right) \quad (3)$$

For the crystalline plane (002), the above eq. (3) reduces into the relation

$$c = \frac{\lambda}{\sin\theta} \quad (4)$$

and the obtained values of 'c' parameter are found to be 5.210, 5.205 and 5.202 Å and the values of the parameter 'a' are found to be 3.256, 3.253 and 3.251 Å for the devices fabricated at 400, 500 and 600 ^{o}C, respectively. A small decrease in lattice parameters' values is observed with annealing temperatures.

The obtained values of the lattice parameters 'a' and 'c' are further used to estimate the volume of the unit cell [22] using the relation

$$V = \frac{\sqrt{3}}{2} a^2 c \qquad (5)$$

And the observed values of the unit cell volumes for different sets of films are presented in Table-1. The effect of annealing temperature on the lattice stress (S) and strain (ε) has also been examined for the deposited films [19-21], using the relations

$$S = \frac{\lambda}{\Delta \sin\theta} - \frac{\beta}{\tan\theta} \qquad (6)$$

and

$$\varepsilon = \frac{\beta \cos\theta}{4} \qquad (7)$$

The obtained values of lattice stress and micro-strain for the n-ZnO thin films obtained at different annealing temperature are tabulated in Table 1. It is found that the values of both stress and strain decreases with increase in annealing temperature. The obtained values of these parameters are well matched with the reported values of the parameters for the deposited ZnO thin films [18-21].

The grain boundary specific surface area (S_a) and theoretical density (D_T) of deposited films are crucial parameters for the surface structure dependent applications like gas sensing, photodetectors, etc. Therefore, the effect of annealing temperature on these parameters has also been investigated. The grain boundary specific surface area (S_a) is estimated [20, 24] using the formula

$$S_a = \frac{1.65}{\Delta} \quad (8)$$

And the theoretical density is estimated [25] using the relation

$$D_T = \frac{2M}{NV} \text{ (in g/cm}^3\text{)} \quad (9)$$

Where, M is the molecular weight, N is Avogadro's number, and V is the volume of the unit cell. The values of these parameters are presented in Table 1. It is found that the value of grain boundary specific surface area decreases, whereas, the density of the films increases with increase in annealing temperature.

Table 1: Structural parameters of the deposited films estimated from XRD patterns

Sample name	n-ZnO/p-Si^{++}at 400 ^{o}C	n-ZnO/p-Si^{++} at 500 ^{o}C	n-ZnO/p-Si^{++} at 600 ^{o}C
Lattice parameter 'c' (Å)	5.210	5.205	5.202
Lattice parameter 'a' (Å)	3.256	3.253	3.251
Defect density 'δ' (m^{-2})	1.97 x10^{15}	1.75 x10^{15}	1.61 x10^{15}
Crystallite size 'Δ'(nm)	22.55	23.88	24.95
Stress 'S' x10^{-3}	2.06	1.96	1.88
Strain 'ε' x10^{-3}	1.55	1.47	1.40
Inter-planer spacing (Å)	2.605	2.602	2.601
Volume (Å^3)	47.83	47.67	47.61
S_a (x10^7 m^{-1})	8.79	8.30	7.88
Density (g/cm^3)	5.65	5.67	5.68

Figure 1(b-d) shows SEM images of the deposited films at different temperatures. It can be seen from the SEM micrographs that the ZnO nanoparticles of size about 200 nm are uniformly

distribution throughout the film surface. However, it is found that the annealed films at 500 and 600 ^{o}C have relatively larger agglomeration of the nanoparticles with respect to the film deposited at 400 ^{o}C. The observed surface structures of thin films at higher temperature are obvious behavior. Such behavior is commonly observed due to fusion of nanoparticles at higher temperatures.

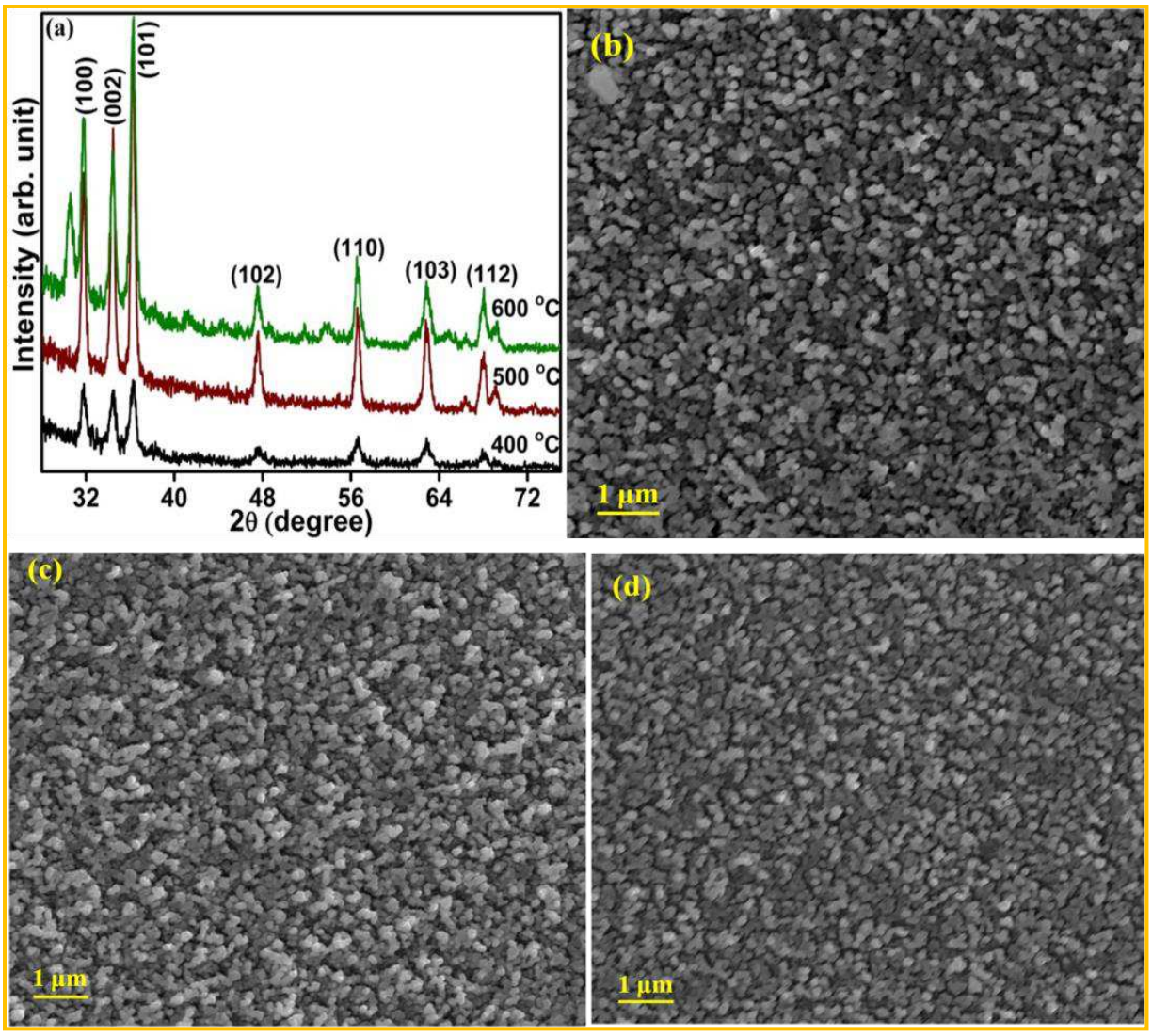

Figure 1 (a) XRD patterns of n-ZnO/p-Si^{++} hetero-junction devices fabricated at 400, 500 and 600 ^{o}C, SEM image of n-ZnO/p-Si^{++} devices fabricated at (b) 400 ^{o}C, (c) 500 ^{o}C and (d) 600 ^{o}C.

3.2. Conduction behavior and hydrogen gas sensing properties

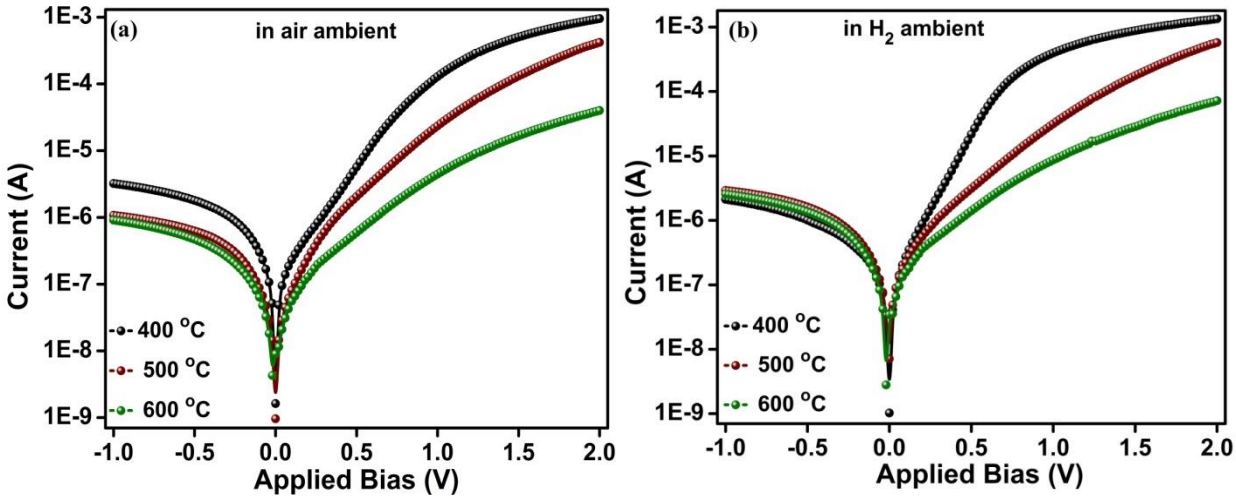

Figure 2 I-V characteristics of the fabricated devices recorded in (a) air ambient and (b) in hydrogen ambient.

Figure 2(a-b) shows the current-voltage (I-V) characteristics of the n-ZnO/p-Si^{++} hetero-junction devices fabricated at different temperatures, recorded in air and hydrogen ambients. It is found that the current flowing through all three hetero-junction devices is non-linear with applied bias voltage. The forward current flowing through the devices increases slowly at lower voltages, say upto to ~0.7 V and then increases very rapidly beyond 0.7 V. However, the current flowing through all the devices in reverse bias condition is almost constant. Such behavior of the hetero-junction devices with applied bias can be attributed to the well-known diodic behavior [26]. It has also been observed that the current flowing through the n-ZnO/p-Si^{++} hetero-junction device fabricated at 400 ^{o}C is greater than the devices fabricated at 500 and 600 ^{o}C. Similar kinds of the behaviors of the fabricated hetero-junction devices with applied bias and annealing temperatures have also been observed in hydrogen ambient. However, a slight increase in current values of the devices has been found in hydrogen environment w.r.t. air ambient. For example, the current values increase from 0.503 mA to 0.879 mA and from 0.131 mA to 0.176 mA at a bias voltage of

1.5 V in the hetero-junction devices fabricated at 400 and 500 ^{o}C, respectively. However, a relative change in current values (I_H/I_a=1.352) of the hetero-junction device fabricated at 500 ^{o}C is lower than the device fabricated at 400 ^{o}C (I_H/I_a=1.748) at room temperature. These values of currents correspond to the percentage sensitivities of 74.93 and 34.18% towards hydrogen gas at room temperature for the devices fabricated at 400 and 500 ^{o}C, respectively i.e. the fabricated devices exhibits significant sensitivity towards hydrogen gas. Thus, to investigate the gas sensing behavior of the fabricated device, the current flowing through the devices at different temperatures in air and hydrogen ambients has been recording. The obtained values of current in hydrogen and air are used to calculate the temperature dependent sensitivity of the fabricated devices using the relation

$$\text{Response}(\%) = \frac{I_{H_2} - I_a}{I_a} \text{x} 100 \qquad (10)$$

Figure 3a shows the temperature dependent sensing response (%) for the hetero-junction device fabricated at 500 ^{o}C. It is observed that the sensitivity of the fabricated device increase with increase in operating temperature upto 100 ^{o}C and decrease beyond this temperature, which is an obvious behavior of the metal oxides. Such temperature dependent behavior of metal oxides can be understood through three physical/chemical processes generally takes place at different temperature. At lower temperatures near room temperature, the physiosorption of oxygen molecules takes place on the film surface [11,27] that can be understood by the processes

$$O_2\,(\text{molecule}) \rightarrow O_2\,(\text{ads. at film Surf.}) \qquad \text{(i)}$$

$$O_2\,(\text{ads at film Surf.}) + e^{-}(\text{pull}) \rightarrow O_2^{-}(\text{ads. at lower temp.}) \qquad \text{(ii)}$$

This process of adsorption of oxygen (O_2) molecules on the film surface and dragged out of electron from film surface to form oxygen ions (O_2^-), results into the generation of a lower conductive region on the film surface called the depletion layer. Larger be the adsorption of

oxygen molecules, more will be the length of depletion layer and lower be the electrical conductivity of the deposited film in air ambient. The surface adsorbed oxygen ions interact with hydrogen gas molecules, in hydrogen ambient. The electrons are returned back to the conduction band that results into the decrease in depletion layer thickness and increase in electric current in hydrogen environment. This caused in an increase in sensing response of the fabricated devices. This process can be understood [9, 11,27] by the relation

$$H_2 + O_2^- \text{ (ads at ZnO Surf.)} \rightarrow H_2O \text{ (ejected as vapor)} + 2e^- \text{ (returned back to C. B.)} \quad \text{(iii)}$$

The length of depletion layer (L_D) depends upon the temperature, which can be given by the relation [28,29]

$$L_D = \sqrt{\left(\frac{\varepsilon_0 kT}{ne^2}\right)} \quad (11)$$

Where, n is the number the charge carriers, ε_0 is the static dielectric constant and other parameters have their usual meanings. At further higher temperature, the physiosorbed oxygen ions (O_2^-) chemically react to each other to form chemisorbed oxygen ions (say O^{2-} or $2O^-$) at film surface. Such processes can be given by [6,11,30,31]

$$O_2 \text{ (ads at ZnO Surf.)} + 2e^- \text{(pull)} \rightarrow 2O^- \text{(ads. in mid} - \text{temp. range)} \quad \text{(iv)}$$

$$O_2 \text{ (ads at ZnO Surf.)} + 4e^- \text{(pull)} \rightarrow 2O^{2-} \text{(ads. at higher temp.)} \quad \text{(v)}$$

In this temperature range, the depletion width has the maximum value. i.e. in this temperature range, there are maximum number of active sites or oxygen ions for compensation by the analyte gas (H_2) molecules. And the process of compensation [10, 27,32] can be rewritten as

$$H_2 + 2O^- \text{(ads. in mid. temp. range)} \rightarrow H_2O \text{ (vapor)} + 2e^- \text{ (returned back to C. B.)} \quad \text{(vi)}$$

The fabricated devices having maximum sensitivity in this temperature range (around 100 ^oC in present case). Beyond a specifically higher operating temperature (>100 ^oC), the fabricated devices or ZnO films show well-known semiconducting behavior in which thickness of the

depletion layer decreases due to increase in charge carrier concentration. And thus, the sensitivity of the fabricated devices decreases beyond a particular temperature.

To investigate the effect of hydrogen concentrations on the sensing response of the fabricated devices, the change in electric current has been recorded at different concentrations of hydrogen ranging from 200 to 1000 ppm at an operating temperature of 100 ^{o}C. Figure 3(b-d) shows the transient sensing response of the fabricated hetero-junction devices at 200, 400, 600, 800 and 1000 ppm of hydrogen. It is found that the sensing responses of the fabricated devices increase with increase of hydrogen concentrations. However, the sensing response of the fabricated devices decreases with increase in annealing temperature. i.e. the observed sensing response of ~97.22% for the device fabricated at 400 ^{o}C decreases to 64.23% for the device fabricated at 500 ^{o}C and finally to ~40.77% for the device fabricated at 600 ^{o}C at 1000 ppm of hydrogen gas. The observed sensing responses of the fabricated devices are of the order or better than the reported values of sensitivity [33-39]. The comparative values for the sensing responses are presented in Table 2. The cyclic response of all three devices at five different concentration of hydrogen suggests the cyclic stability and repeatability of the fabricated devices.

The transient gas sensing response of the fabricated devices can be understood by adsorption kinetic of the gas molecules on the surface of the sensing device. One of the such adsorption kinematics was introduced by the Langmuir's based upon the homogeneity of the surface. Some basic assumptions of this theory are that (i) the adsorbing surface should be homogeneous, (ii) the adsorbing surface contains some specific number of actives sites, which are available for adsorption, each site can only accommodate only one gas molecule and as such as each site is occupied by the analyte gas (i.e. if one monolayer completes), no further adsorption takes place [40,41]. This assumption corresponds to the saturation of gas sensing response with

time, and (iii) all the sites are equivalent and independent i.e. the presence of other molecules do not affect the occupancy (energy of adsorption) of newly arriving molecule. However, this theory of the homogeneous surface was later modified by Freundlich for the heterogeneous surfaces and semiconducting materials [40-42]. Since, the surface morphology/structure of the deposited films strongly dependent on the deposition techniques and process conditions i.e. temperature and pressure, etc. Thus, the discontinuity and heterogeneity of the film surface is obvious, which results into the non-uniform adsorption of the analyte gas molecules.

Table 2: Comparative sensing responses of the fabricated devices

S. No.	Device structure	H_2 Conc. (ppm)	Response (%)	Operating temperature (^oC)	Ref.
1	rGO/ZnO Hetero-junction	500	96%	-----	[6]
2	MXene/SnO_2 Hetero-junction	50	40%	------	[7]
3	n-ZnO/p-NiO Hetero-junction	100	53%	237	[33]
4	Au/ZnO Schottky	1000 (~1%)	48%	210	[34]
5	ZnO@SnO_2 Resistive	500	70%	400	[35]
6	ZnO-SnO_2 Resistive	1000	45%	200	[36
7	ZnO Resistive	1000	43%	150	[37]
8	Ni-ZnO-rGO	100	63.8%	150	[50]
9	ZnO resistive	150	6	400	[51]
10.	n-ZnO/p-Si Hetero-junction	1000	97%	100	[This work]

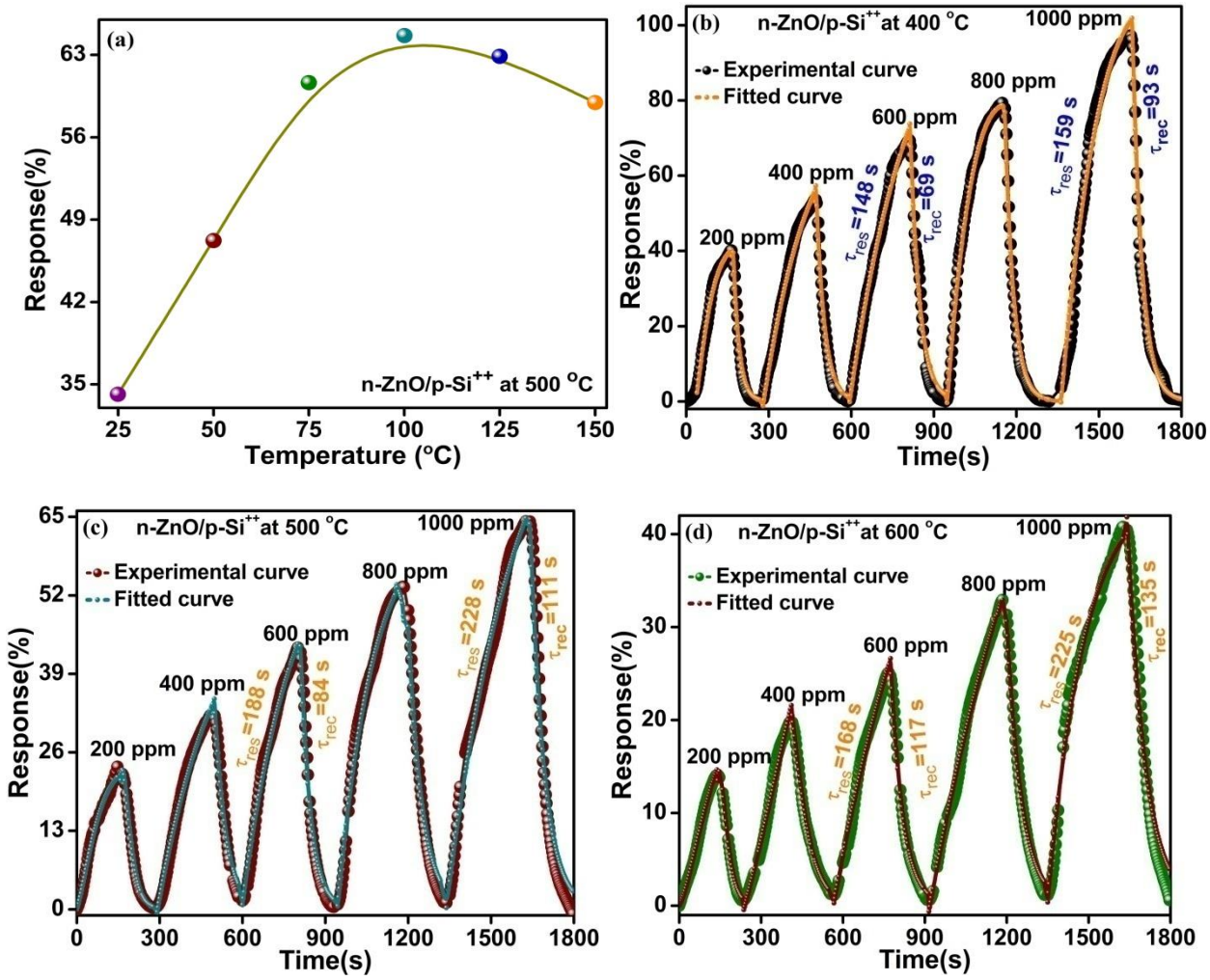

Figure 3 (a) Temperature dependent sensing response of the device fabricated at 500 °, transient sensing response of the fabricated devices at (b) 400 °C (c) 500 °C and 600 °C recorded at different hydrogen concentrations (200 to 1000 ppm)

Therefore, the transient gas sensing response of the present devices can be determined by the modified Freundlich adsorption isotherm for the non-uniform adsorption of hydrogen molecules and/or desorption of oxygen molecules in hydrogen ambient. Thus, the rise in sensing responses of the fabricated devices in hydrogen environment with time can be fitted with modified Freundlich relation for the desorption of oxygen molecules or adsorption of hydrogen molecules [40,41], given by

$$R = R_{a1}\left(1 - e^{-t/\tau_{a1}}\right) + R_{a2}\left(1 - e^{-t/\tau_{a2}}\right) \quad (12)$$

Where, R_{a1} and R_{a2} are the pre-exponential factors of the rising of sensing response, and τ_{a1} and τ_{a2} are the time constants for sensing response.

Table 3: Freundlich's fitting parameters for the adsorption of hydrogen molecules for the fabricated hetero-junction devices

Sample Name	**H_2 (ppm)**	**200**	**400**	**600**	**800**	**1000**
n-ZnO/p-Si at 400°C	R_{a1}	-15415.39	-72680.49	-168481.88	-257432.82	-459208.62
	τ_{a1}	32.23	105.69	159.68	251.29	330.76
	R_{a2}	15458.22	72757.69	168593.62	257371.23	393541.26
	τ_{a2}	32.39	106.25	160.82	248.73	343.64
	Exactness	0.99441	0.99299	0.99591	0.99215	0.97887
n-ZnO/p-Si at 500°C	R_{a1}	-15366.33	-39411.16	-35432.76	-1655033.79	-277424.40
	τ_{a1}	41.61	122.65	136.05	110.70	212.84
	R_{a2}	15390.92	39461.04	35496.10	1655098.05	277519.44
	τ_{a2}	41.65	123.29	140.31	113.07	218.69
	Exactness	0.9919	0.98827	0.98833	0.99057	9918
n-ZnO/p-Si at 600°C	R_{a1}	-32946.50	-233004.16	-1227706.57	-1228786.19	-1018930.76
	τ_{a1}	69.22	287.51	222.51	303.95	86.15
	R_{a2}	32969.81	233100.17	1227762.32	1228857.59	1018976.04
	τ_{a2}	69.26	287.69	222.55	304.06	134.64
	Exactness	0.99541	0.98476	0.98817	0.99435	0.98618

Table 4: Freundlich's fitting parameters for the desorption of hydrogen molecules for the fabricated hetero-junction devices

Sample Name	**H_2 (ppm)**	**200**	**400**	**600**	**800**	**1000**
n-ZnO/p-Si at 400°C	R_{d1}	52975.1	13.48 x10^{7}	62.02 x10^{10}	2.17 x10^{17}	3.34x10^{23}
	τ_{d1}	21.59	30.65	34.52	31.93	31.75
	R_{d2}	55920.2	13.49 x10^{7}	63.01 x10^{10}	2.17 x10^{17}	2.99 x10^{21}
	τ_{d2}	21.58	30.66	34.51	31.93	35.93
	Exactness	0.97782	0.97555	0.97137	0.98439	0.99336
n-ZnO/p-Si at 500°C	R_{d1}	-15.78 x10^{6}	29.33 x10^{5}	52.75 x10^{9}	33. x10^{10}	2.74 x10^{15}
	τ_{d1}	18.48	41.39	36.59	51.02	51.14
	R_{d2}	14.45 x10^{6}	29.22 x10^{5}	12.46 x10^{10}	42.90 x10^{10}	2.73 x10^{15}
	τ_{d2}	18.69	41.40	36.61	51.02	51.15
	Exactness	0.99716	0.95882	0.97399	0.97401	0.95029
n-ZnO/p-Si at 600°C	R_{d1}	-45.83 x10^{5}	-72.96 x10^{7}	30.09 x10^{7}	33.12 x10^{9}	1.25 x10^{12}
	τ_{d1}	18.44	37.94	45.72	55.81	66.13
	R_{d2}	43.02 x10^{5}	72.42 x10^{7}	30.11 x10^{7}	33.12 x10^{9}	1.25 x10^{12}
	τ_{d2}	18.61	37.97	45.71	55.82	66.12
	Exactness	0.99494	0.99758	0.98613	0.98285	0.94829

Whereas, on the removal of hydrogen gas molecules from the sensing cavity, the adsorption of the oxygen molecules starts and the sensing device approaches to its original state. The current flowing through the device falls during the desorption of hydrogen gas molecules or adsorption of

oxygen molecules and corresponding decrease in sensing response. Thus, the transient decay of sensing response is fitted with the modified Freundlich's equation for the desorption of hydrogen molecules or adsorption of oxygen molecules, given by [40,41]

$$R = R_{d1}\left(e^{-t/\tau_{d1}}\right) + R_{d2}\left(e^{-t/\tau_{d2}}\right) \quad (13)$$

Where, R_{d1} and R_{d2} are the pre-exponential factors for decaying sensing response. τ_{d1} and τ_{d2} are the time constants for decaying sensing response.

The transient rising and decaying sensing responses of the fabricated devices are fitted with eq. (12) and (13), respectively. And the fitting parameters for the rise and decay in sensing responses are presented in Table 3 and Table 4, respectively. It is found that the eqs. (12) and (13), very well fit the response and recovery parts of the transient sensing behaviors of all the fabricated devices.

The transient sensing response curves have also been used to calculate the response (τ_{res}) and recovery (τ_{rec}) times for different cycles recorded at different hydrogen concentrations as shown in Fig 3(b-d). It is found that the response and recovery times increase with increase in hydrogen concentration as well as fabrication temperature. The values of response time increase from 84 to 159 s, 126 to 228 s and 144 to 225 s on changing the hydrogen concentration from 200 to 1000 ppm for the devices fabricated at 400, 500 and 600 ^{o}C, respectively. Similarly, the values of recovery time increase from 51 to 93 s, 85 to 111 s and 88 to 135 s on changing the hydrogen concentration from 200 to 1000 ppm for the devices fabricated at 400, 500 and 600 ^{o}C, respectively. The lower value of recovery times as compared to response times for all the fabricated devices discards the possibility of strong chemical reaction (or absorption) of hydrogen gas molecules on the film surface. Thus, simple adsorption-desorption processes can be attributed to the mechanism of gas sensing in these devices.

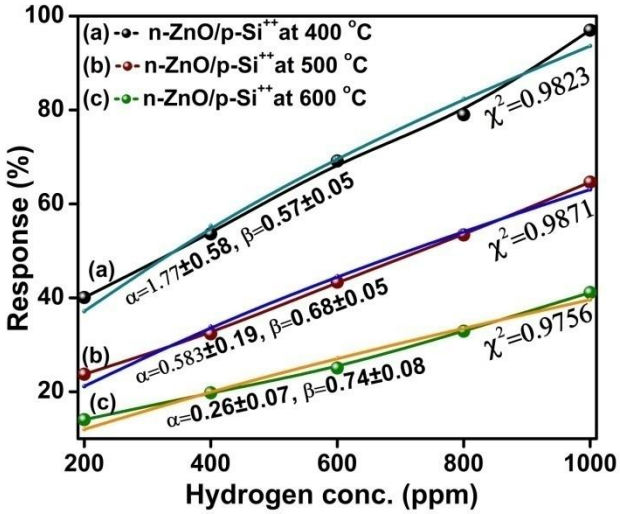

Figure 4 Sensing responses (%) of the fabricated devices as a function of hydrogen concentration with corresponding Freundlich's fitted curves.

Figure 4 shows the sensing response of the fabricated hetero-junction devices as a function of hydrogen concentration. It is found that the gas sensing responses of all three devices increase almost linearly with hydrogen concentration. The gas sensing response of the fabricated devices as a function of analyte gas concentration can also be understood in terms of Freundlich's relation given by [40,42,43]

$$\text{Response} \propto \alpha C^{\beta} \qquad (14)$$

where, α and β are the Freundlich's undeterminants related with the surface structures and β can have value between 0 and unity, C is the concentration of analyte gas (say H_2 in present case). The beauty of eq. (14) is that this equation accounts for the heterogeneity of the deposited films. However, there is an incongruity with this model is that Freundlich's isotherm tends to infinity as C tends to infinity. i.e. there is no restriction of the adsorption of gas molecules on the film surface or in a monolayer. This results into the infinitely rising in sensing response of the fabricated device with analyte gas concentration, which is unphysical. Thus, a modified Freundlich's eq. could be good choice to explain the concentration dependent gas sensing

responses of the device. The modified Freundlich's eq. for concentration dependent gas sensing response can be given by [40,42,43]

$$\text{Response} \propto \frac{\alpha C^{\beta}}{1+\alpha C^{\beta}} \quad (15)$$

For the lower concentrations of the analyte gas, the above eq. (15) reduces into the eq. (14), whereas, for very high concentrations, R.H.S. of eq. (15) approaches to 1 and gas sensing response approaches to a constant/saturated value. Thus, concentration dependent gas sensing responses of the deposited films are fitted with eq. (15) and the obtained values of α and β for the fabricated devices are shown in Figure 4 along with the goodness of fitting. It is found that all the curves are very well fitted with Freundlich's relation with goodness of fitting better than 97.5%. Furthermore, the value of β-parameters increases from 0.57±0.05 to 0.68±0.05 and to 0.74±0.08 on increasing the fabrication temperature from 400 to 500 ^{o}C and to 600 ^{o}C, respectively. The increase in β-parameter with fabrication temperature can be attributed to the faster saturation of gas sensing response i.e. accommodation of lower number of analyte gas molecules in the first monolayer or lower active sites in case of device fabricated at higher temperature.

3.3. Mechanism of gas sensing in hydrogen environmental

The mechanism of hydrogen sensing (i.e. change in electric current) in n-ZnO/p-Si^{++} hetero-junction devices fabricated at different temperatures can be further understood by three more elegant models such as space charge region current control model (ii) grain boundary specific surface area and potential barrier height current control model and (iii) valence state current control model [11]. The current controlled by these three processes under hydrogen environment can be analyzed one by one, as follows

(i) Space charge region current control model: according to this model, in air ambient, oxygen (O_2) molecules are adsorbed on the active sites of film surface (Fig. 5a) and dissociated into two

atomic oxygen atoms at moderate temperature (say 100 ^{o}C in present case) to occupy two active sites [11,44] The electrons are transferred to these atomic oxygen atoms (Fig. 5b) via reaction mechanism (iv) and thus, the electrons are depleted from the grains and grain boundary regions (or from the conduction band) near the upper surface of the films. This electron depleted region is called space charged or depletion region as shown in Fig. 5c. The reduced electrons' concentration in depletion region results into the decrease in electrical current (conductivity) flowing through the hetero-junction devices in air ambient. The length of this lower conductive region (L_D-Debye length) can be given by eq. (11), which is an inverse function of carrier concentration. Thus, the decrease in carrier concentration means larger the thickness of this region and hence, lower the conductivity of the fabricated devices when measured in air ambient (Fig. 2a).

On the other hand, in hydrogen ambient, the reaction mechanism of type eq. (vi) will take place. The electrons are become free and returned back to the conduction band, which means an increase in carrier concentration and hence decrease in the thickness of depletion layer. This ultimately results into the increase in electric current flowing through the hetero-junction devices in hydrogen environment and responsible for hydrogen gas sensing. This process can be understood shematically through Fig. 5 (d-e). In hydrogen environment, H_2 molecules adsorbed on the active sites on the film surface (Fig 5d) and these adsorbed H_2 molecules interact with oxygen ions of the depletion layer (Fig. 5e) to form H_2O molecules which are evaporated at the operating temperature (Fig. 5f) and electrons are given back to the film. This results into the decrease in the thickness of depletion layer, as can be depicted from Fig. 5f.

Larger the number of grains and grain boundaries means larger the active sites for interaction. Thus, a decrease in gas sensing response of the hetero-junction devices with increase in

fabrication temperture from 400 to 600 ^{o}C can be attributed to the decrease in number of grains and grain boundaries as observed from the increase in crystallites' size and grain boundaries specific surface area measured from XRD patterns. Furthermore, the observed density of the fabricated films from XRD studies also found to increase with fabrication temperature, which means lower penetration of hydrogen molecules into the bulk of films. This again cause a decrease in the number of active sites for interaction and hence, the lower sensitivity of the devices fabricated at higher temperatures.

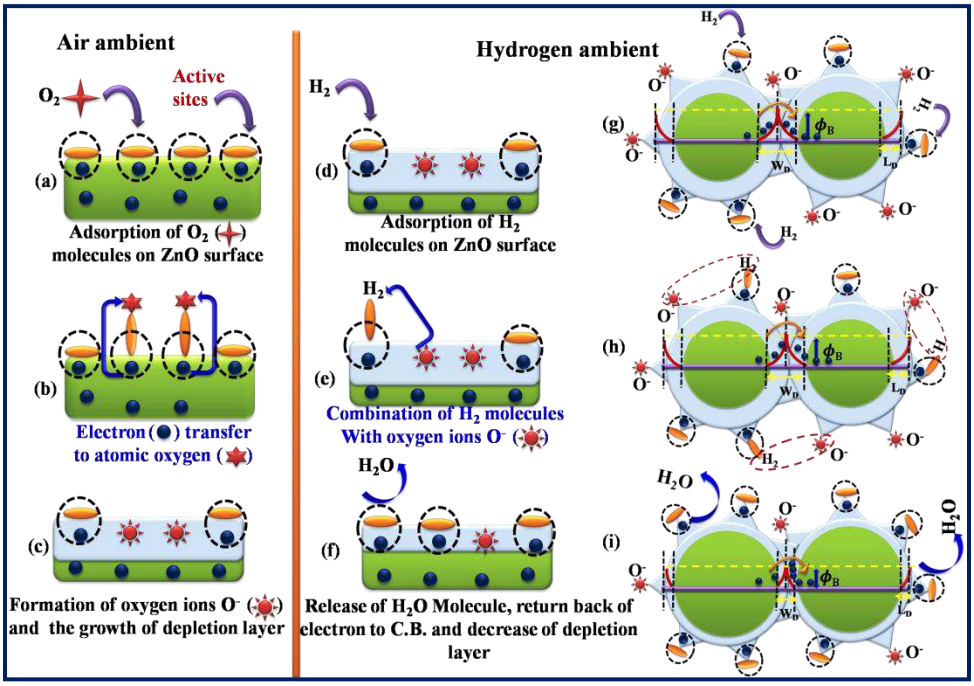

Fig. 5 Schematic demonstration of the interaction of n-ZnO/p-Si^{++} hetero-junction device with air and hydrogen ambients, and corresponding change in the electronic states of deposited films, (a) exposure of film surface with environment oxygen, (b) dissociation of O_2 molecules and adsorption on active sites in ionic form, (c) development of depletion layer on transfer of electrons to the atomic oxygen in air ambient, (d) interaction of depleted film films with H_2 molecules in hydrogen ambient, (e) combination of H_2 molecules with ionic atomic oxygen and (f) ejection of water molecules from film surface at operating temperature and release of electron

to the film surface causing a decrease in depletion layer thickness, (g) exposure of grain boundaries to the hydrogen gas and the representation of potential barriers at the grain boundaries, (h) interaction of H_2 molecules with oxygen ions to form H_2O molecules near the grain boundaries and (i) the evaporation of water molecules resulting in decrease in depletion width at the grain boundaries and the corresponding decrease in potential barrier height.

Grain boundary current control model: The growth of the lower conductive space charge region upon the capriciously scattered ZnO grains results into the development of potential barriers between two grains [45,46] (i.e. at the grain boundaries) as shown in Fig. 5g. For the transport of the charge carriers (i.e. electrons), carriers have to jump over this potential barrier or crossover the grain boundaries (inset of Fig. 5g). Thus, the electrical properties or the current flowing through the fabricated devices is determined by the height of the potential barrier or the contact resistance between of the grains [47] and given by relation

$$I = I_o \exp\left\{\frac{-e\phi_B}{kT}\right\} \quad (16)$$

Where, I_o is the pre-exponential factor referred as the current flowing through the device at zero Kelvin and ϕ_B is the potential barrier height, which is related with the width of depletion layer (W_D) at the grains boundaries by the relation

$$W_D = \sqrt{\left(\frac{2\epsilon_0\phi_B}{N_d e^2}\right)} \quad (17)$$

Where, N_d is the donor density and ε_0 is the permittivity of free space.

The value of the potential barrier height for the fabricated devices can be estimated using the Richardson's relation, wherein the reverse saturation current and the potential barrier height are inter-related by the expression

$$I_0 = AA^*T^2 \exp\left(-\frac{e\phi_B}{kT}\right) \quad (18)$$

where, A* is the Richardson's constant having the value of =32 $Acm^{-2}K^{-2}$ and A is the area of Pt electrodes (=0.785 cm^2). And the obtained values of the potential barrier height estimated in air ambient for the devices fabricated at 400, 500 and 600 ºC are 0.402, 0.425 and 0.434 eV, respectively. The increase in potential barrier height with annealing temperature is attributed to the corresponding decrease in electric current flowing through the devices.

On the other hand, the values of the potential barrier height decrease in hydrogen environment to 0.384, 0.409 and 0.421 eV for the devices fabricated at 400, 500 and 600 ºC, respectively. The H_2 molecules interacts with oxygen ions to form H_2O molecules near the grain boundaries (Fig. 5h) and the water molecules are evaporated from the film surface resulting in decrease in depletion width at the grain boundaries (Fig. 5i) and a corresponding decrease in potential barrier height is observed. The decrease in potential barrier height is the responsible factor for the observed increase in electric current in hydrogen environment. Thus, the proportionate change in potential barrier height ($\Delta\phi_B$=0.018, 0.016 and 0.013 eV) in hydrogen ambient is responsible for the relative in change in electric current and given by

$$I_R = I_o \exp\left\{\frac{-e\Delta\phi_B}{kT}\right\} \quad (19)$$

Lower the change in potential barrier height means lower the sensing response as observed for the devices fabricated at higher temperature.

Valence state controlled current conduction: A third mechanism that can contribute in the gas sensing response of the fabricated devices is the valence state current control mechanism. According to this mechanism, because of high reducing ability of hydrogen gas, on exposure of the ZnO surface with hydrogen gas molecules, the ZnO molecules reduce into the Zn^+ ions. In this process Zn^+ ions are introduced into the ZnO surface that produced metallization effect and change the valence state of Zn [11, 48,49]. This effect drastically increases the electrical

conductivity of the fabricated device. However, metallization effect generally occurs at relatively higher temperatures and thus can have only a small contribution in the electrical gas sensing measured at 100 ^{o}C in the present case. Thus, the major contribution in hydrogen gas sensing comes from the earlier mechanisms.

4. Conclusion

In summary, the hetero-junction devices based on n-ZnO/p-Si^{++} were fabricated at three different temperatures of 400, 500 and 600 ^{o}C. For the fabrication of these devices, ZnO thin films were grown by thermal evaporation techniques, wherein, high quality Zn dust was evaporated slowly on the highly doped p-type silicon substrates maintained at 400 ^{o}C. Other two sets of films were obtained after annealing the deposited films at 500 and 600 ^{o}C. The structural analysis carried out under x-ray diffraction revealed that the crystallite size, grain boundary specific surface area and the density of the films increases with increase in fabrication temperature. I-V characteristics of the fabricated hetero-junction devices showed non-linear diodic behaviors in air and hydrogen gas environments. I-V characteristic of the fabricated devices also revealed the increase in electric current, when the devices are exposed to hydrogen environment. The fabricated hetero-junction devices are further analyzed for the hydrogen detection under different concentrations (200 to 1000 ppm) of hydrogen. It is found that the gas sensing response of the fabricated devices increase with increase in operating temperature (up to 100 ^{o}C) as well as the hydrogen concentration. However, the sensing response of the fabricated devices decreases from 97.22 to 64.23 and to 40.77 % with increase in annealing temperature from 400 to 500 and to 600 ^{o}C at 1000 ppm of hydrogen in ambient air. The sensing response of the device fabricated at 400 ^{o}C is found to increase from ~40.07 to 97.22% and for the device fabricated at 500 ^{o}C from 23.73 to 64.23 on increasing the hydrogen concentration from 200 to 1000 ppm in air ambient. The

mechanism of gas sensing has been systematically analyzed under space charge region control, grain boundaries control and valence state control current conduction. The values of response time increase from 84 to 159 s, 126 to 228 s and 144 to 225 s on changing the hydrogen concentration from 200 to 1000 ppm for the devices fabricated at 400, 500 and 600 ^{o}C, respectively. Similarly, the values of recovery time increase from 51 to 93 s, 85 to 111 s and 88 to 135 s on changing the hydrogen concentration from 200 to 1000 ppm for the devices fabricated at 400, 500 and 600 ^{o}C, respectively.

Acknowledgement

Authors are thankful to Director, SRM-Institute of Science and Technology, Ghaziabad, UP for providing necessary research facilities for present work.

Ethics approval: The work presented here authors original work. Contributions of all the workers are declared here. No animal or human being harmed during this work.

Consent to participate: Not Applicable

Consent for publication: Not Applicable

Availability of data and materials: Data will be provided on request.

Competing interests: The authors declare that they have no known competing financial interests or personal relationships that could have appeared to influence the work reported in this paper.

* **Funding:** No funding is received for this work from any agency.

Authors' contributions:

Vinod Kumar: Writing- Original draft preparation, Reviewing and Editing

Ishpal Rawal: Supervision, Conceptualization, Validation, Software, Reviewing and Editing

Vipin Kumar: Data collection, Methodology, Visualization

Authors' information (optional): Not Applicable

Disclosure of potential conflicts of interest: The authors declare that there are no any kinds of conflicts of interest to declare.

Research involving Human Participants and/or Animals: No Human or animal participant were involved by any of authors for this work.

Informed consent: Not Applicable

References

[1]. Lu Y, Huang J., Li B., Tang K., Ma Y., Cao M., Wang L., Wang L. (2018), Appl. Surf. Sci. **428**: 61–65.

[2]. Yu X., Chen H., Ji Q., Chen Y., Wei Y., Zhao N., Yao B (2021) Chemosphere **267**: 129285

[3]. Yatskiv R., Tiagulskyi S., Grym J., Vanis J., Basinova N., Horak P., Torrisi A., Ceccio G., Vacik J., Vrňata M. (2020) Thin Solid Films **693:**137656.

[4]. Cao Y.Q., Qian X., Zhang W., Wang S.S., Li M., Wu D., Li A. D (2017) J. Electrochem. Soc. **164:** A3493

[5]. Chang C. M., Hon M. H., Leu I. C (2013), J. Electrochem. Soc. **160**: B170.

[6]. Drmosh Q.A., Hendi A.H., Hossain M.K., Yamani Z.H., Moqbel R.A., Hezam A., Gondal M A (2019) Sens. Actuat. B **290:** 666–675.

[7]. He T., Liu W., Lv T., Ma M., Liu Z., Vasiliev A., Li X (2021) Sens. Actuat. B **329**: 129275.

[8]. Tai H., Duan Z., He Z., Li X., Xu J., Liu B., Jiang Y (2019) Sens. Actuat. B **298**:126874.

[9]. Mustaffa S.N.A., Ariffin N.A., Khalaf A.L., Yaacob M.H., Tamchek N., Paiman S., Sagadevan S.(2020) J. Mater. Res. Technol. **9**:10624–10634.

[10]. Kim J.H., Mirzaei A., Osada M., Kim H. W., Kim S S (2021) Sens. Actuat. B **329**: 129222.

[11]. Ren Q., Cao Y.Q., Arulraj D., Liu C., Wu D., Li W.M., Li A D (2020) J. Electrochem. Soc. **167:**067528

[12]. Seiyama T., Kato A., Fujiishi K., Nagatani M (1962) Anal. Chem. **34**:1502-1503.

[13]. Weichsel C., Pagni O., Leitch A W R (2005) Semicond Sci. Technol. **20**:840.

[14]. Sypien B. L., Czapla A., Lubecka M., Kusior E., Zakrzewska K., Radeck M., Kusior A., Balogh A.G., Lauterbach S., Kleebe H J (2013) Sens. Actuators B **187**: 445–454.

[15]. Nguyen D.D., Do D.T., Vu X.H., Dang D.V., Nguyen D C (2016) Adv. Nat. Sci. Nanosci. Nanotechnol. **7**: 015004.

[16]. Meng W., Dai L., Zhu J., Li Y., Meng W., Zhou H., Wang L (2016) Electrochim. Acta **193**: 302–310.

[17]. Choi J. H., Park T., Hur J., Cha H Y(2020) Sens. Actuat. B **325**: 128946 (1-8).

[18]. Ashwini J., Aswathy T.R., Nair A S (2021) Biochem. Biophy. Reports **26**:100995.

[19]. Rawal I (2015) RSC Adv. **5**:4135-4142.

[20]. Singh K., Rawal I., Gautam P., Sharma N., Dhar R (2018) J. Magn. Magn. Mater. **468**:259–268.

[21]. Zak A.K., Abd. Majid W.H., Abrishami M.E., Yousefi R (2011) Solid Stat. Sci. **13**: 251-256.

[22]. Ahmed M. M. A., Tawfik W. Z., Elfayoumi M. A. K., Abdel-Hafiez M., El-Dek S I (2019) J. Alloys Compd. **791**: 586–592.

[23]. Singh K., Rawal I., Sharma N., Gautam P., Dhar R (2019) Mater. Sci. Semicond. Process. **95**:7–19.

[24]. Straumal B.B., Protasova S.G., Mazilkin A.A., Tietze T., Goering E., Schütz G., Straumal P.B., Baretzky B (2013) Beilstein J. Nanotechnol **4**: 361-369.

[25]. Rani S., Ahlawat N., Kundu R. S., Punia R., Kumar S., Sangwan K. M., Ahlawat N (2017) Ferroelectrics **516**: 156–166

[26]. Mohammed YH (2019) Superlatt. Microstruct. **131**: 104–116.

[27]. Pal P., Yadav A., Chauhan P. S., Parida P. K., Gupta A (2021) Sens. Internat. **2**: 100072

[28]. Lupan O., Chow L., Pauporte T., Ono L.K., Cuenya B. R., Chai G (2012) Sens. Actuat. B **173**: 772– 780

[29]. Mirzaei A., Kim J.H., Kim H. W., Kim S S (2018) Sens. Actuat. B **258**: 270-294

[30]. Khun K. K., Mahajan A., Bedi R K (2009) J. Appl. Phys. 106:124509

[31]. Gautam M, Jayatissa A H (20120 J. Appl. Phys. **112**: 114326.

[32]. Kim J.-H., Mirzaei A., Kim H.W., Kim S. S (2019) Sens. Actuat. B **284**: 628-637.

[33]. Nakate U. T., Ahmad R., Patil P., Wang Y., Bhat K. S., Mahmoudi T., Yu Y.T., Suh E. K., Hahn Y B (2019) J. Alloy. Compd. **797**: 456-464

[34]. Pandis C., Brilis N., Bourithis E., Tsamakis D., Ali H., Krishnamoorthy S., Iliadis A A (2007) IEEE Sensors J. 7**:** 448-454

[35]. Tien L.C., Norton D.P., Gila B.P., Pearton S.J., Wang H.T., Kang B S (2007) Appl. Surf. Sci. **253:** 4748-4752.

[36]. Mondal B., Basumatari B., Das J., Roychaudhury C., Saha H., Mukherjee N (2014) Sens. Actuat. B Chem. **194**: 389-396

[37]. Rout C. S., Krishna S.H, Vivekchand S. R. C., Govindaraj A., Rao C. N. R (2006) Chem. Phys. Lett. **418**:586-590.

[38]. Bhati V.S., Ranwa S., Rajamani S., Kumari K., Raliya R., Biswas P., Kumar M (2018) ACS Appl. Mater. Interfaces **10**:11116–11124.

[39]. Drmosh Q.A., Yamini Z.H., Hossain M K (2017) Sens. Actuat. B **248**: 868-877

[40]. Gautam M., Jayatissa A. H (2012) J. Appl. Phys. **111**: 094317.

[41]. Pal R., Goyal S. L., Rawal I., Sharma S (2020) Iran. Polym. J. **29**:591–603.

[42]. Hu H., Trejo M., Nicho M.E., Saniger J.M., Gracia-ValenZuela A (2002) Sens. Actuat. B **82:** 14-23.

[43]. Johnson J. L., Behnam A., An Y., Pearton S. J., Yral A. (2011) J. Appl. Phys. **109**: 124301.

[44]. Kim J.-H., Mirzaei A., Kim H.W, Wu P., Kim S. S (2019) Sens. Actuat. B **293**: 210-223.

[45]. Nulhakim L., Makino H., Kishimoto S., Nomoto J., Yamamoto T (2017) Mater. Sci. Semicond. Process. **68:**322-326

[46]. Katoch A., Abideen Z. U., Kim H. W., Kim S. S (2016) ACS Appl. Mater. Interfaces **8:**2486-2494.

[47]. Shi Y., Wang M., Hong C., Yang Z., Deng J., Song X., Wang L., Shao J., Liu H., Ding Y (2013) Sens. Actuat. B **177:** 1027– 1034.

[48]. Lupan O., Postica V., Labat F., Ciofini I., Pauporté T., Adelung R (2018) Sens. Actuat. B **254:**1259-1270.

[49]. Weber M., Kim J.-H., Lee J.-H., Kim J.-Y., Iatsunskyi I., Coy E., Drobek M., Julbe A., Bechelany M., Kim S. S (2018) ACS Appl. Mater. Interfaces **10**: 34765-34773.